Charge Transport Mechanism in Intercalated Polypyrrole Aluminum-Pillared Montmorillonite Clay Nanocomposites

Abdul Shakoor,[1] Tasneem Zahra Rizvi,[2] Maryam Hina[1]

[1]*Department of Physics, Bahauddin Zakariya University, Multan, Pakistan*
[2]*Physics Department, Quaid-i-Azam University, Islamabad, Pakistan*

Received 9 April 2011; accepted 27 July 2011
DOI 10.1002/app.35432
Published online 21 November 2011 in Wiley Online Library (wileyonlinelibrary.com).

ABSTRACT: Nanocomposites based on intercalated conducting polypyrrole (PPy) into the galleries of inorganic aluminum-pillared Montmorillonite (Al-PMMT) clay with varying concentrations of Al-PMMT were prepared by *in situ* chemical polymerization. The intercalation was confirmed by X-ray diffraction pattern. Charge transport mechanism in these composites was investigated by temperature dependent direct current conductivity measurements. An increase in DC conductivity value on addition of (Al-PMMT) clay in the composites at all temperatures and a transition from three-dimensional (3D) Mott's variable range hopping (VRH) process in pristine PPy to one-dimensional (1D) Mott's VRH process in the intercalated polymer composites has been observed. This transition in charge transport mechanism of PPy from 3D VRH to 1D VRH on intercalation has been interpreted in terms of straightening and linearization of polymer chains and decrease in inter-chain interactions in the intercalated PPy. Enhancement in mechanical properties and increase in thermal stability of the nanocomposites was also observed with the increase in weight percentage of Al-PMMT in PPy-Al-PMMT composites. © 2011 Wiley Periodicals, Inc. J Appl Polym Sci 124: 3434–3439, 2012

Key words: conducting polymers; electron microscopy; electrical properties; thermogravimetric analysis

INTRODUCTION

Conducting polymer/clay nanocomposites exhibit new synergistic properties, which cannot be attained from individual materials. Conductivity is more easily controlled, and the mechanical or thermal stability is improved through the synthesis of the nanocomposites.[1] Composites of conducting polymers and nanostructured clays have also shown promise as conductive fillers in insulating polymers.[2] Many researchers have reported increasing conductivity with increasing wt% of nonconducting materials like Y_2O_3[3] and MMT.[4] Pillared-layered clays are novel materials, which possess several interesting properties, such as large surface area, high pore volume, and tunable pore size (from micropore to mesopore), high thermal stability, strong surface acidity, and catalytic active substrates/metal oxide pillars.[5] The authors have recently reported synthesis of intercalated polypyrrole aluminum-pillared Montmorillonite (PPy-Al-PMMT) nanocomposites, which exhibited marked increase in their room temperature AC and DC conductivities[6] with the increase of Al-PMMT content in the nanocomposites. The present study investigates the difference in charge transport mechanisms in pristine polypyrrole (PPy) and its clay nanocomposites to find out the cause of increased electrical conductivity in these nanocomposites when compared with pristine PPy. The prospective nanocomposites have further been characterized by transmission electron microscopy (TEM), thermogravitational analysis (TGA), and mechanical behavior.

Correspondence to: A. Shakoor (shakoor_47@yahoo.com).

Journal of Applied Polymer Science, Vol. 124, 3434–3439 (2012)

EXPERIMENTAL

Materials

Pyrrole was purchased from Fluka, aluminum-pillared montmorillonite clay (Al-PMMT), and $FeCl_3.6H_2O$ was provided by Aldrich. Pyrrole was freshly distilled before use. All materials were used as provided without any further purification. Preparation of PPy and PPy-aluminum-pillared clay composites PPy-Al-PMMT as given below was according to already reported method[5].

Preparation of polypyrrole

An amount of 5.404 g of $FeCl_3.6H_2O$ was dissolved in 10 mL of distilled water and stirred for 1 h. A total of 2.683 g pyrrole was dropped slowly in the suspension during stirring. The suspension was left 24 h for polymerization.[2] Finally, the suspension was filtered and washed with distilled water again

and again to remove $FeCl_3.6H_2O$ and other adhering substances. Greenish-black powder of PPy was obtained which was dried at 90°C for 24 h in a vacuum oven.

Preparation of PPy-aluminum-pillared clay composites

For the synthesis of PPy-Al-PMMT clay composites in aqueous medium, the Al-PMMT clay dispersion in aqueous medium was first prepared by adding known weights of Al-PMMT (2.683 g) clay into known volume of distilled water (10 mL) under constant stirring. After 1 h, $FeCl_3.6H_2O$ (5.404 g) was added to the dispersion in such a way that it would attain the required concentration. Pyrrole was then added into the dispersion so as to make 2 : 1 mole ratio of $FeCl_3.6H_2O$ to pyrrole under constant stirring at room temperature (25°C). The total volume of the reaction mixture was kept at 50 mL. The gradual change of color from light black to deep greenish-black indicated the formation of PPy. The reaction mixture was then kept under room temperature for 24 h. The resulting deep greenish-black mass was filtered and then it was thoroughly washed with distilled water until it was completely free from $FeCl_3$. This process was repeated several times to remove all adhering substances. Finally, the product was washed with water again and then it was dried at 90°C for 24 h to yield a very fine deep greenish-black powder of PPy-Al-PMMT clay composite. All the samples were kept desiccated prior to measurements.

Measurements

Powder X-ray diffraction (XRD) patterns were obtained in the range of 2θ (2–10°) using X-Ray Diffractometer featuring Cu K_α (λ = 1.5406 Å) radiations, working voltage 40 kV and working current 30 mA. Conductivity measurements were made in pressed pellets of approximately 3 mm thickness prepared in 13 mm diameter stainless steel die under 10 ton pressure in a SPECAC KBr press under vacuum. The electrical conductivity was measured by conventional four probe and the samples were connected to a Keithley 617 programmable electrometer and Keithley 224 sourcemeter. The TGA was carried out on Mettler thermo balance STAR S.W. 8.10 from room temperature (25°C) to 800°C for all the samples. The samples were heated at the rate of 10°C/min in nitrogen atmosphere. SEM images of samples were obtained using Scanning Electron Microscope JEOL-Japan, Model JSM 5910 up to the magnification of 10,000 at an operating voltage of 5 kV. TEM was carried out with Philips CM12 microscope at accelerating voltage of 80 kV. TEM micrograph was obtained in a very thin film obtained by dropping the solution on the surface of water and then fishing it on the grid. The grid was kept under vacuum to evaporate solvent for 24 h at room temperature. Instron mechanical tester was used for the measurement of mechanical properties of the materials.

RESULTS AND DISCUSSION

X-ray diffraction patterns of Pure PPy, pure Al-PMMT, and their composites are shown in Figure 1. As the major crystalline peaks in XRD of Al-PMMT are also present in the XRD of all the composite samples, it is evident that the Al-PMMT is not exfoliated or delaminated to a large extent in the composite samples. Insertion of the PPy into the layers of clay was also examined by XRD. According to the well known Bragg's law $\{n\lambda = 2d \sin\theta\}$, where n is an integer, λ is the X-ray wavelength, d is the distance between crystal lattice planes, and θ is diffraction angle, the crystalline peak at 2θ value of 4.6 in pure Al-PMMT sample corresponds to the periodicity d = 1.9 nm in the direction of (001) of the clay samples. This basal (d 001) peak was shifted toward higher angles in PPy-Al-PMMT nanocomposites because of the intercalation of PPy, which replaces Al pillars from the inter layer clay galleries during nanocomposite synthesis. As a result, the d-spacing in the direction of (001) of the pillared clay samples is reduced to a value of 1.73 and 1.47 nm in the composite samples with 10 and 15% Al-PMMT, respectively.

DC conductivity measured in pure PPy and in its composites with 10, 15, and 25% Al-PMMT clay is given in Table I, as a function of weight percentage of Al-PMMT clay. Increase in the conductivity of the composites was observed with the increase of clay content, which was rapid for upto 25% clay. This increase in conductivity is attributed to the straightening of the PPy chains due to intercalation in the

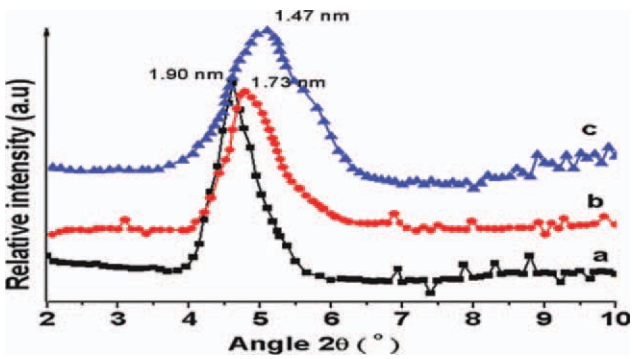

Figure 1 XRD pattern of (a) pure Al-PMMT Composite of PPy with (b) 5%Al-PMMT, (c) 10.0%Al- PMMT. [Color figure can be viewed in the online issue, which is available at wileyonlinelibrary.com.]

TABLE I
DC Conductivity and *d*-Values of PPy-Al-PMMT Clay Composites

Sample	*d*-Values (nm)	Conductivity (S cm^{-1})
Pure PPy		3.9×10^{-2}
10.0% Al-PMMT in PPy	1.47	4.8×10^{-2}
15.0% Al-PMMT in PPy	1.73	4.9×10^{-2}
Pure Al-PMMT	1.90	$\sim 10^{-9}$ (Aldrich)

interlamellar galleries of the pillared clay. The relationship between applied voltage and current obtained for various samples were also studied, which showed the ohmic behavior.

The relation between the DC conductivity and temperature on the polymer sample can give important information concerning the nature of the phenomena related to the charge transport in a polymer system. According to Mott's variable range hopping (VRH) mechanism of charge transport the following relations are taken into consideration[7–9]:

$$\sigma = \sigma_o \exp\left(-\frac{T_o}{T}\right)^{\frac{1}{1+n}} \quad (1)$$

In this study, σ_o and T_o are the pre-exponential factor and Mott's characteristic temperature and can be obtained from the intercepts and slopes of log(σ) vs. $T^{-1/n+1}$. The density of states at Fermi level, hopping length, and hopping energy can be calculated using eqs. (2)–(5):

$$\sigma_0 = e^2 R^2 \upsilon_{ph} N(E_F) \quad (2)$$

$$T_0 = \frac{\lambda \alpha^3}{kN(E_F)}[\mathrm{K}] \quad (3)$$

$$R = \left[\frac{9}{8\pi\alpha kTN(E_\mathrm{F})}\right]^{1/4}[cm] \quad (4)$$

$$W = \frac{3}{4\pi R^3 N(E_\mathrm{F})}[\mathrm{eV}] \quad (5)$$

where σ = conductivity of sample at temperature T(K), σ_0 = pre-exponential factor (S cm^{-1}), T_0 = characteristic temperature (K), e = electronic charge (1.602×10^{-19}C), k = Boltzmann's constant (8.616×10^{-5} eV K^{-1}), R = average hopping distance (cm), υ_{ph} = phonon frequency ($\sim 10^{13}$ Hz), $N(E_\mathrm{F})$ = density of localized states at the Fermi level (cm^{-3} eV^{-1}), λ = dimensional constant ($\sim$ 18.1), α = coefficient of exponential decay of the localized states (cm^{-1}), W = average hopping energy (eV), $\alpha^{-1} = L$, which is the localized length and its value is estimated from monomer Pyrrole length 3 Å.[10,11]

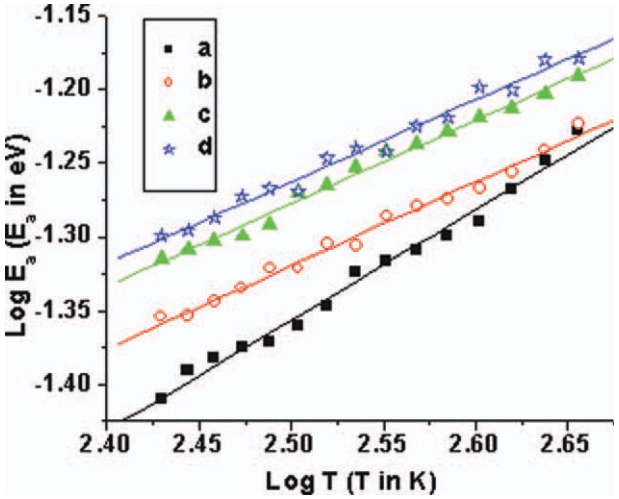

Figure 2 Graph of log(E_a) vs. log T of (a) PPy, (b) 10% Al-PMMT, (c) 15% Al-PMMT, and (d) 25% Al-PMMT clay in PPy. [Color figure can be viewed in the online issue, which is available at wileyonlinelibrary.com.]

To explicitly determine the mechanism of charge transport, the conductivity data have been analyzed in term of Mott's VRH model the exponent n in eq. (1) is the dimensionality of mechanism, its value can be n = 1, 2, or 3 for 1D, 2D, or 3D VRH charge transport mechanism, respectively. The value of n can be determined from the temperature dependence of activation energy. The activation energy E_a is given by eq. (6):

$$E_\mathrm{a} = \frac{d(\mathrm{Log}\ \sigma)}{d\left(\frac{1}{kT}\right)} \quad (6)$$

So the activation energy can be calculated from the slope of log σ vs. $1/T$. and can be exploited to find the hopping mechanism of charge transport. By

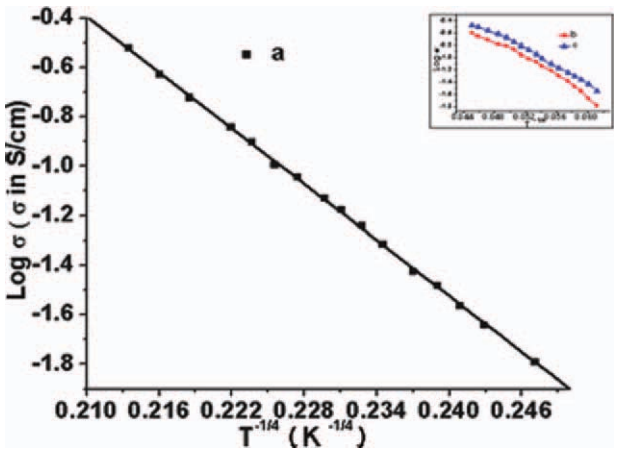

Figure 3 Graph of log(σ) vs. $T^{-1/4}$ of (a) PPy and in inset is graph of log(σ) vs. $T^{-1/4}$ of (b) 10% and (c) 15% Al-PMMT clay in PPy. [Color figure can be viewed in the online issue, which is available at wileyonlinelibrary.com.]

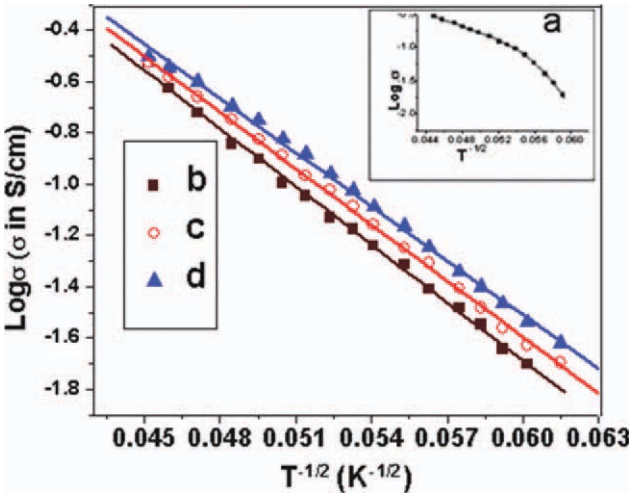

Figure 4 Graph of log(σ) vs. $T^{-1/2}$ of (b) 10% (c) 15% Al-PMMT and (d) 25% clay in PPy and in inset is graph of log(σ) vs. $T^{-1/4}$ of (a) PPy. [Color figure can be viewed in the online issue, which is available at wileyonlinelibrary.com.]

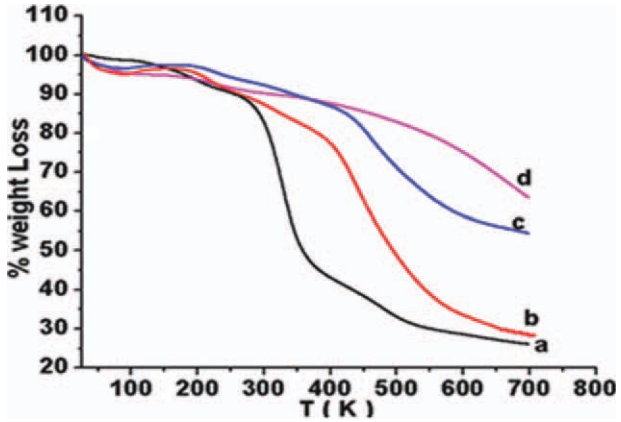

Figure 5 TGA curves of (a) PPy, (b) 10%, (c) 15% Al-PMMT clay in PPy, and (d) pure Al-PMMT clay. [Color figure can be viewed in the online issue, which is available at wileyonlinelibrary.com.]

combining eqs. (1) and (6), obtained the following eq. (7).

$$E_a = \gamma k T_o \left(\frac{T_o}{T}\right)^{\gamma-1} \quad (7)$$

where $\gamma = \frac{1}{1+n}$, by plotting log (E_a) vs. log T (Fig. 2), a straight line of the plot of log (E_a) vs. log T (Figure 2a) and a straight line of slope $\{-(\gamma - 1)\} = 0.75$ is obtained for pristine PPy, which corresponds to hopping exponent $\gamma = 1/4$ and $n = 3$, which shows that 3D VRH is dominant in pristine PPy. On the contrary, for PPy-Al-PMMT clays samples, the plot of log(E_a) vs. log T [Figure 2(b–d)] gives straight lines of slope $\{-(\gamma - 1)\} = 0.55$ to 0.56, which corresponds to hopping exponent $\gamma = 0.5 \pm 0.05$ and $n \sim 1$. This indicates that the 1D VRH dominates the mechanism of charge transport in the PPy-Al-PMMT nanocomposites. From these results, the authors said that the charge transport mechanism is switched from 3D VRH in case of pristine PPy to 1D VRH in all PPy-Al-PMMT clay samples. This indicates comparatively a smaller number of inter-chain links and hence a lower rate of inter-chain charge carrier hopping when compared with intra-chain hopping in the nanocomposites. The observed increase in the conductivity of the nanocomposites with Al-PMMT clay loading can also be explained in terms of fast 1D charge carrier hopping along the straightened and less inter-linked chains of intercalated PPy in the nanocomposites. Temperature dependent log of conductivity was also found to have a linear relationship with $T^{-1/4}$ in case of pure PPy (Fig. 3) and was found to have a linear relationship with $T^{-1/2}$ in case of composites of PPy-Al-PMMT clay (Fig. 4). In set Figure 3 shows the graph of log(σ) vs. $T^{-1/4}$ of (b) 10% and (c) 15% Al-PMMT clay in PPy, which shows that log(σ) vs. $T^{-1/4}$ is no more linear but is in polynomial fit with Order 3. In set Figure 4 shows the graph of log(σ) vs. $T^{-1/2}$ PPy, which shows that log(σ) vs. $T^{-1/4}$ is no more linear, which also confirmed that the charge transport mechanism of pristine PPy follows the 3D VRH model and that of composites follow 1D VRH model as described by eq. (1). The best-fitted Mott's parameters σ_o, density of states at Fermi level, hopping length, and activation energy as defined in eqs. (2)–(7) were calculated and given in Table II. The pre-exponential factor σ_o was found to increase with the increase in weight percentage of Al-PMMT clay in PPy, whereas the Mott's characteristic temperature T_o and hopping length were found to increase with Al-PMMT clay concentration

Figure 5 shows typical TGA curves of the PPy and PPy-Al-MMT composites. The TGA curve of PPy

TABLE II
Mott's Parameters of PPy-Al-PMMT Clay Nanocomposites

Samples	Density of states $N(E_f)$	Hopping length (Å)	Hopping energy (eV)	σ_o (S cm^{-1})
PPy	4.6×10^{21} (eV^{-1} cm^{-3})	15.01	0.055	1.32×10^2
10%	6.6×10^{12} (eV^{-1} cm^{-1})	10.5	0.033	4.51×10^3
15%	6.9×10^{12} (eV^{-1} cm^{-1})	10.1	0.030	4.798×10^3
25%	7.3×10^{12} (eV^{-1} cm^{-1})	9.47	0.027	5.134×10^3

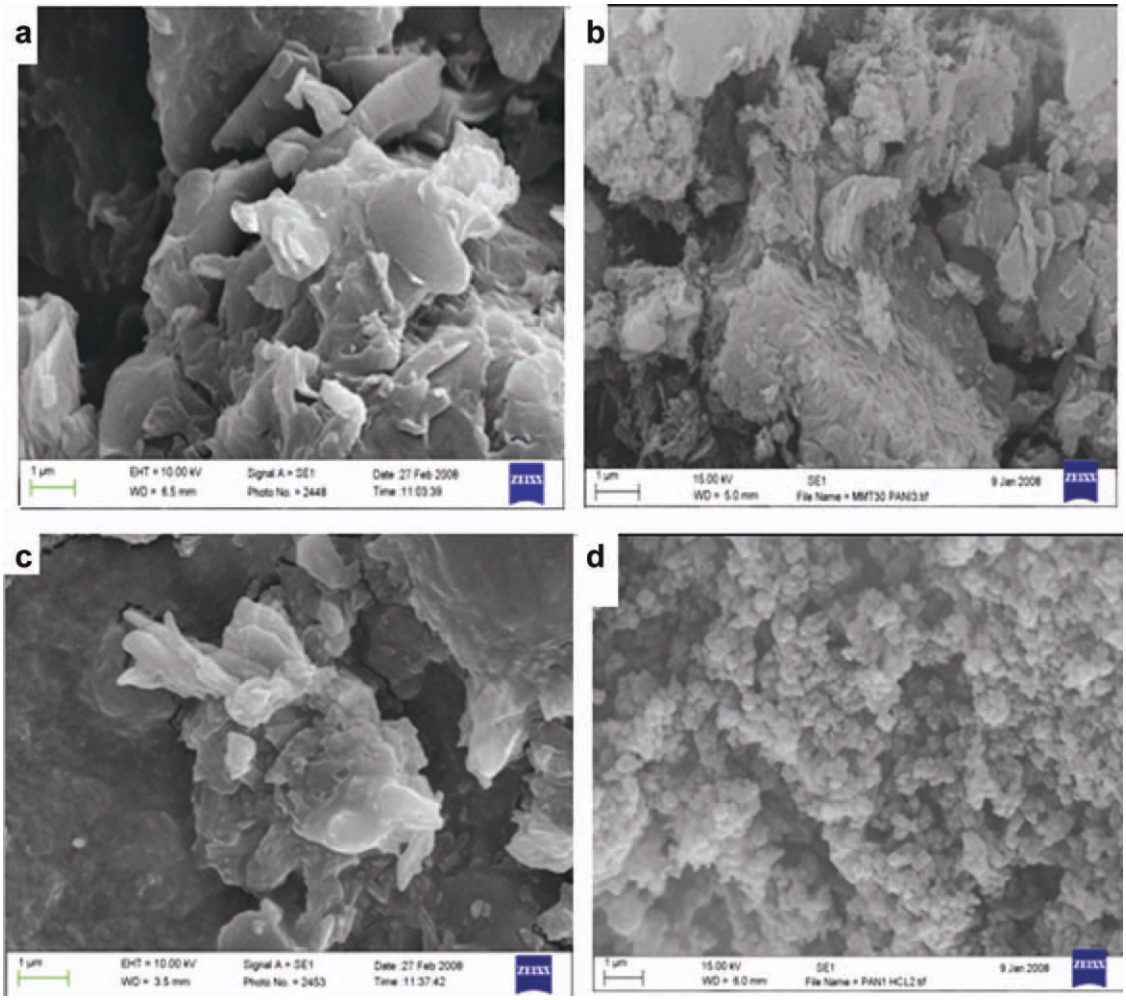

Figure 6 SEM micrographs of (a) pure PPy, (b) 10% Al-PMMT-PPy composite, (c) 25% Al-PMMT-PPy composite, and (d) pure Al-PMMT. [Color figure can be viewed in the online issue, which is available at wileyonlinelibrary.com.]

exhibited two stages of weight loss, the first stage starts from 180°C and the percentage weight loss is 5%, second degradation starts at 350°C, and the percentage degradation process is referred to organic compound in pure PPy weight loss is 15%. This onset of the thermal decomposition in all the nanocomposites like that found in pristine PPy at 180°C is absent in all the composite samples, which shows that rapid thermal decomposition does not occur in the nanocomposites even up to 500°C. There is however some gradual weight loss in all the composites, which is found to decrease with the increase of Al-PMMT percentage in the composites.

Figure 6(a–d) shows SEM micrographs of pure Al-PMMT clay, nanocomposites of PPy containing 10 and 15% Al-PMMT clay and pure PPy, respectively. As is evident from these micrographs pure Al-PMMT exhibits a platy morphology [Fig. 6(a)], whereas the pure PPy exhibits submicron sized globular morphology [Fig. 6(d)]. Both the nanocomposites with 10% [Fig. 6(b)] and 25% [Fig. 6(c)] Al-PMMT clay in PPy exhibit morphologies that resemble more with that of pure Al-PMMT clay and are very different from that of pure PPy. This shows that the clay is either intercalated between the clay galleries or is aligned on the external surfaces of the clay particles to give rise to

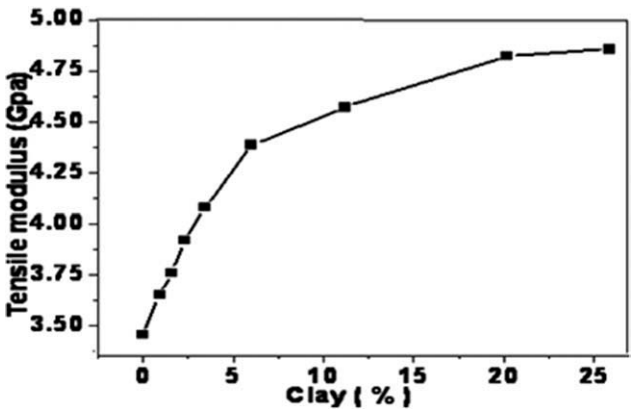

Figure 7 Effect of clay loading on tensile modulus.

a platy morphology instead of the globular morphology of the pristine PPy.

Mechanical properties are shown in Figure 7. Enhancement in mechanical properties was observed in polymer nanocomposites, which are also attributed to the intercalation of PPy into the layers of Al-PMMT clay. It may be noted that, in contrast to intercalation, exfoliation process does not have a considerable effect on the mechanical properties of the composites.[12,13] The enhanced mechanical properties, dimensional stability, together with thermal stability of the intercalated PPy-Al-PMMT nanocomposites make these materials promising for device applications.

Aluminum-pillared clay (Al-PMMT) based nanocomposites of PPy were successfully obtained by chemical polymerization in the presence of $FeCl_3$ in aqueous medium. The pyrrole is polymerized into the layers of Al-PMMT forming a regular aligned chains of PPy, which not only enhances AC and DC conductivities as has been observed but also the mechanism of conduction is switched on from 3D VRH in case of pristine PPy to 1D VRH in all PPy-Al-PMMT nanocomposites. The intercalation of PPy into the layers of Al-PMMT clay was also confirmed by XRD and TEM. TGA curves showed that the thermal stability is enhanced by insertion of PPy in Al-PMMT clay layers. Enhanced Mechanical properties are also attributed to intercalation of PPy into the layers of Al-PMMT clay.

Authors gratefully acknowledge the financial support from Higher Education Commission, Pakistan.

References

1. Kim, J. W.; Liu, F.; Choi, H. J.; Hong, S. H.; Joo. J. J. Polymer 2003, 44, 289.
2. Omastova, M.; Mravcàkova, M.; Pionteck, J.; Chodak, I. Conf. Proc-Nanocomposites, San Francisco, CA: USA. October 9–12, 2003.
3. Vishnuvardhan, T. K.; Kulkarni, V. R.; Basavaraja, C.; Raghavendra, S. C. Bull Mater 2006, 29, 77.
4. Anuar, K.; Murali, S.; Fariz, A.; Ekramul, H. N. J Mater Sci 2004, 10, 253.
5. Ding, Z.; Kloprogge, J. T.; Frost, R. L.; Lu, G. Q.; Zhu, H. Y. J Porous Mater 2001, 6, 273.
6. Shakoor, A.; Anwar, H.; Rizvi, T. Z. J Composite Mater 2008, 42, 10.
7. Mott, N.; Deies, E. Electronic Progress in Noncrystalline Materials; Clarendon Press: Oxford, 1997, 94, 174.
8. Jonscher, A. K. Nature; London, 1977, 253, 717.
9. Louati, B.; Gargouri, M.; Guidara, K.; Mhiri, T. J Phys Chem Solids 1999.
10. Maddison, D. S.; Tansley, T. L. J Appl Phys 1992, 72, 4677.
11. Saunders, B. R.; Murray, K. S.; Flemming, R. J. Synth Met 1992, 1, 329.
12. Ma, J.; Yu, Z.-Z.; Kuan, H.-C.; Dasari, A.; Mai, Y.-W. Macromol Rapid Commun 2005, 26, 753.
13. Okada, A.; Usuki. A. Mater Sci Eng 1995, C3, 109.